Tackling Issues of Lithium Metal Anodes with a Novel Polymeric Lithicone Coating

Xin Wang[a], Jiyu Cai[b], Kevin Velasquez Carballo[a], Fumiya Watanabe[c], and Xiangbo Meng[a,*]

[a] Department of Mechanical Engineering, University of Arkansas, Fayetteville, AR 72701, USA

[b] Chemical Sciences and Engineering Division, Argonne National Laboratory, Lemont, IL 60439, USA

[c] Center for Integrative Nanotechnology Sciences, University of Arkansas at Little Rock, AR 72204, USA

*Corresponding author: xbmeng@uark.edu

Abstract

Lithium metal (Li) has been hindered from as anodes in commercial batteries for over 50 years, due to two main issues: continuous formation of solid electrolyte interphase (SEI) and lithium dendritic growth. In this work, we report a new strategy to tackle these issues, i.e., using molecular layer deposition (MLD) to grow an ionically conducting but electrically insulating polymeric lithicone coating, an Li-containing triethanolamine (LiTEA). Our electrochemical tests revealed that this LiTEA coating could serve as an exceptional protection layer over Li anodes. Consequently, the LiTEA-coated Li electrodes could achieve a superior cyclability of > 10000 Li stripping/plating cycles at a current density of 5 mA cm^{-2} and a long cyclability of > 5500 cycles at 2 mA cm^{-2} in Li‖Li symmetric cells without failures, under a fixed areal capacity of 1 mAh cm^{-2}. Characterizations using scanning electron microscopy and X-ray photoelectron microscopy verified that Li^+ ions could be easily extracted through and deposited under the LiTEA coating during the stripping/plating processes. Consequently, this LiTEA coating significantly inhibited the formation of SEI and Li dendrites. This underlies the long cycling lifetime of the LiTEA-coated Li‖Li cells. Coupling with the nickel-rich $LiNi_{0.8}Mn_{0.1}Co_{0.1}O_2$ (NMC811) cathodes, more encouragingly, the LiTEA-coated Li anodes could remarkably extend the cyclability and sustainable capacity of the resultant Li‖NMC full cells. We also demonstrated that the performance of Li‖NMC cells could be further improved through combining an LiTEA-coated Li anode with an Li_2S-modified NMC811 via atomic layer deposition (ALD). Thus, this study is inspiring for developing high-energy Li‖NMC lithium metal batteries.

Keywords: Lithium metal batteries, lithium metal anodes, molecular layer deposition, atomic layer deposition, solid electrolyte interphase, lithium dendrites, and surface coating.

1. Introduction

The market share of battery-powered electric vehicles (BEVs) has been increasing in recent years, but is still very low, less than 10% worldwide. Such a situation is far from our pursuit for a fully electrified society and significantly destined due to the multiple insufficiencies of state-of-the-art lithium-ion batteries (LIBs) in energy density, cost, safety, and lifetime. Featuring the adoption of lithium metal (Li) as their high-capacity anodes (3860 mAh g^{-1}) [1-5], in this context, lithium metal batteries (LMBs) are highly regarded as a successor of LIBs enabling much higher energy density for BEVs to reach extended driving range. Coupling with different cathodes, several prototypes of LMBs are undergoing intensive investigation. Among them, $LiNi_{0.8}Mn_{0.1}Co_{0.1}O_2$ (NMC811) is very attractive, ascribed to its low cost, high capacity, and high voltage. However, the resultant Li||NMC811 LMBs suffer from a series of issues rooted in their Li anode and NMC811 cathode, which hinder them from commercialization. On the cathode side, NMC811 suffers from a series of issues including microcracking [6, 7], irreversible phase transition [8], oxygen release [8, 9], metal dissolution [10], and residual lithium compounds (LiOH, Li_2O, and Li_2CO_3) [11]. On the anode side, Li metal mainly experiences two challenges: (1) continuous formation of unstable solid electrolyte interphase (SEI) and (2) lithium dendritic growth [1, 12]. In tackling these issues, surface coating is a common strategy widely practiced on both the cathode and anode. The resultant effects of the coatings are closely related to their quality and properties. In this regard, atomic and molecular layer deposition (ALD & MLD) are two emerging thin-film

deposition techniques enabling various coatings accurately in a layer-by-layer growth mode. They exhibit a series of inherent merits while share a highly analogous growth mechanism. Through adopting different precursors, ALD specially grows inorganic films with an accuracy at the atomic level while MLD particularly enables organic films precisely at the molecular level [1, 2, 13, 14]. Consequently, they both deliver high-quality coatings at low temperatures (e.g., ≤ 150 °C). In recent years, there have been an increasing number of A/MLD efforts invested for surface coatings of Li||NMC LMBs.

Our recent efforts have investigated a number of surface coatings via ALD [15-18]. Among them, we for the first time have revealed that sulfides are a promising class of coating materials for tackling the issues of NMC811 [15]. This discovery has been demonstrated with the nanoscale Li_2S coating via ALD (i.e., ALD-Li_2S). Our study disclosed that the ALD-Li_2S coating has played multiple functional roles: (1) mechanical strengthener, (2) interface and structure stabilizer, and (3) oxygen scavenger. All these are significant for boosting the performance of NMC811. Particularly, it is unique that Li_2S was found to react with oxygen released from NMC811 and then transformed into Li_2SO_3 or/and Li_2SO_4. This transformation not only improved the ionic conductivity of the coating layer but also protected electrolytes from oxidation. As a consequence, the Li_2S-coated NMC811 enabled a much better performance than the bare one, accounting for a capacity retention of ~71% vs. ~11% after 500 charge-discharge cycles, respectively.

Along with our efforts on the NMC cathodes, recently we also have reported that MLD is a viable technique for designing lithicones (e.g., LiGL, GL = glycerol) as ionically conductive coatings of Li anodes. The resultant MLD-coated Li anodes exhibited exceptional cyclability in Li||Li symmetric cells [1]. Inspired by the excellent protective

effects of these lithicones, we have been continuing our search for new lithicones as the novel coatings of Li anodes and this study was part of our on-going efforts. In this study, we report a new lithicone by MLD using lithium *tert*-butoxide (LTB, i.e., LiO^{t}Bu) and triethanolamine (TEA, i.e., $N(CH_2CH_2OH)_3$) as precursors and demonstrate its exceptional protective effects on Li anodes. We found that the resultant LiTEA lithicone enabled long-term cyclability of Li‖Li symmetric cells. Furthermore, we revealed that coupling the LiTEA-coated Li anode with the Li_2S-coated NMC811 enabled the best performance of Li‖NMC811 cells. In this study, consequently, we report for the first time that the combination of both ALD and MLD can best address the issues existing with Li‖NMC LMBs. This study indicated that it is critical to tackle the issues of both the Li anode and NMC cathode simultaneously for achieving the most desirable performance of LMBs.

2. Results and discussion

Fig. 1a illustrates the MLD process of the LiTEA lithicone, using LTB and TEA as precursors. The resultant LiTEA is highly tunable in its thickness through simply adjusting the MLD cycle number. This could be well demonstrated and measured using an *in situ* quartz crystal microbalance (QCM), as also described in our previous studies [1, 19, 20]. To establish a repeatable surface for growing LiTEA on the QCM crystal, we pre-deposited a layer of Al_2O_3 film on the crystal using ALD (inset of Fig. 1b). The continuous mass gain in the QCM profile verified that the paired LTB/TEA precursors are feasible for growing LiTEA lithicone (Fig. 1b and 1c). The MLD QCM profile in Fig. 1b reveals that the LiTEA growth on the Al_2O_3 film is nearly linear after an initiation stage of ~10 MLD cycles having a lower growth per cycle (GPC). The stable LiTEA

MLD growth has a relatively constant GPC, as shown in Fig. 1c, in which the doses of LTB and TEA are signified by two different colored bars. Each dose of these two precursors caused some mass gain (as shown in Fig. 1c), i.e., m_1 and m_2 due to LTB and TEA, respectively. The total mass gain of each MLD cycle ($\Delta m = m_1 + m_2$) is measured as ~45 ng cm^{-2} cycle^{-1} in the stable growth region.

To determine the GPC in Å cycle^{-1}, we further deposited LiTEA films over nitrogen-doped graphene nanosheets (N-GNS) (Fig. 2a) at 150 °C. The N-GNS features its high surface area and thin wrinkles of < 3 nm [1, 21]. Observing the thickness changes of the N-GNS wrinkles after the LiTEA deposition of 100 and 200 MLD cycles using scanning electron microscopy (SEM), we could conclude that the average GPC of the MLD LiTEA is ~3.6 Å cycle^{-1}.

We further postulated the overall reaction of the MLD LiTEA as follows in Equation 1:

$$3LiO^tBu + N(CH_2CH_2OH)_3 \rightarrow N(CH_2CH_2OLi)_3 + 3HO^tBu \quad (1)$$

This reaction indicates that the LiTEA has a unit structure of $N(CH_2CH_2OLi)_3$. To verify this postulation, we conducted X-ray photoelectron spectroscopy (XPS) measurements on the composition of the deposited LiTEA films on Si wafers. In Fig. 2b, the Li 1s XPS spectra show only one peak at 56.0 eV, ascribed to Li-O [22]. The N 1s spectra exhibit one peak at 402.0 eV, assigned to N-C or oxidized nitrogen compound [23, 24]. The C 1s spectra show two evident peaks at 285.4 and 284.1 eV, due to C-N/C-OH [25-27] and Li-O-C [28]. The two weak peaks at 288.5 and 287.9 eV are related to O=C-OH [26, 27] and N-C=O/C=O bonds [26, 27, 29]. The O 1s spectra show two peaks at 529.5 eV and 530.8 eV, owing to O^{2-} in Li-O bonds [22, 30, 31] and a peak at 531.5 eV attributed to C-O-Li

[28, 32] or adsorbed H_2O [33]. Our XPS analyses revealed that the deposited LiTEA film contains 16.7 at.% of Li, 5.8 at.% of N, 37 at.% of C, and 40.5 at.% of O. The atomic ratio of Li, N, and C is consistent to our postulation on the LiTEA unit structure $N(CH_2CH_2OLi)_3$, i.e., nearly 3:1:6. We also noticed that there is a higher O content than that of our postulated unit structure. This might be due to some H_2O adsorbed in the LiTEA film during the sample loading process. In addition, synchrotron-based X-ray diffraction (XRD) measurements disclosed that the LiTEA film grown on N-GNS has no peaks observed (Fig. S1 in Supplementary Information), indicating an amorphous nature of the MLD-deposited LiTEA.

To explore the protective effects of this novel LiTEA coating on Li anodes, we deposited it uniformly on Li chips with varying coating thicknesses by tuning the MLD process to 40, 80, 100, 200, 300, 400, and 500 cycles. The resultant MLD-coated Li anodes were then named as **LiTEA-40**, **LiTEA-80**, **LiTEA-100**, **LiTEA-200**, **LiTEA-300**, **LiTEA-400**, and **LiTEA-500**, respectively. We then assembled these LiTEA-coated Li electrodes with the same coating thickness into Li||Li symmetric coin cells and investigated their electrochemical cycling performance, compared with bare Li||Li cells. Under a fixed areal capacity of 1 mAh cm^{-2}, these different Li||Li cells were tested for their Li-stripping/plating cyclability at two different current densities of 2 and 5 mA cm^{-2}. Our results revealed that, at 2 mA cm^{-2} (Fig. 3a), an LiTEA coating of > 40 MLD cycles (~14 nm) is necessary to achieve a desirable protection. Comparable to the bare Li||Li cell, the LiTEA-40||LiTEA-40 cell could only survive for less than 500 cycles. This might be due to its thin coating layer. Both of these two cells evolved in their overpotentials increasing quickly from ~50 to 160 mV in less than 400 Li-stripping/plating cycles. In contrast, both

149 the LiTEA-80||LiTEA-80 and LiTEA-100||LiTEA-100 cells could achieve exceptional
150 cyclability up to 5500 Li-stripping/plating cycles without any failure (Fig. 3a and Fig. S2).
151 They exhibited a highly similar evolution in overpotential, which was relatively high at
152 the first cycle, ~100 mV, but stabilized at ~30 mV after 700 Li-stripping/plating cycles.
153 Very encouragingly, a further increase in the LiTEA coating film thickness could still
154 accomplish stable cyclability in all the cases up to 500 MLD cycles (~180 nm) but only
155 varied the stabilized overpotentials in 5500 Li-stripping/plating cycles (Fig. 3a). We
156 noticed that the LiTEA-200||LiTEA-200 realized the lowest stabilized overpotential of
157 ~20 mV while the stabilized overpotentials increased to ~50, ~85, –and ~100 mV for the
158 LiTEA-300||LiTEA-300, LiTEA-400||LiTEA-400, LiTEA-500||LiTEA-500 cells,
159 respectively (Fig. 3a). These results indicated that, in terms of the stabilized overpotential,
160 there is an optimal coating thickness for the LiTEA film, i.e., LiTEA-200 (~72 nm). A
161 thinner coating might not protect Li anodes well while a thicker coating could hinder the
162 transport of Li^+ ions through the coating layer.

163 At a much higher current density of 5 mA cm^{-2}, our results also verified that the LiTEA
164 coating is compelling and helped Li||Li cells achieve long-term stable cyclability (Fig.
165 3b). As the control, the bare Li||Li cell could only sustain a low overpotential of < 80 mV
166 for only 800 Li-stripping/plating cycles. Thereafter, its overpotential quickly increased up
167 to 1.0 V after ~1300 Li-stripping/plating cycles, indicating a failure of the cell cycling.
168 The LiTEA-40||LiTEA-40 cell could improve its cyclability to a limited extent,
169 sustaining a comparable overpotential of < 80 mV in the first initial 1000 Li-
170 stripping/plating cycles. Thereafter, the cell overpotential increased significantly and
171 reached ~300 mV upon the completion of 2000 cycles, where the cell was regarded a

failure. In contrast, the LiTEA-80||LiTEA-80 and LiTEA-100||LiTEA-100 cells showed little evolution in their cycling overpotential and could sustain a low overpotential of ~80 mV for over 10000 Li-stripping/plating cycles without any failure. Similarly, the LiTEA-200||LiTEA-200 cell could enable a stable but lower overpotential of 68 mV after 10000 Li-stripping/plating cycles without any failure. In addition, Li||Li symmetric cells with thicker LiTEA coatings (LiTEA-300, 400, and 500) still could realize stable long-term cyclability without failures, but just increased the cell overpotential to some extent and sustained an overpotential of 82, 95, and 99 mV after 10000 cycles, respectively, compared to the LiTEA-200||LiTEA-200 cell. Particularly, all these LiTEA-coated cells with a coating of ≥ 80 MLD cycles are still under testing without any failures. These results in Fig. 3a and 3b commonly indicate that the LiTEA-200 is optimal for achieving the best cell performance, in terms of cell overpotential.

Our electrochemical results in Fig. 3 clearly revealed that the Li||Li cells with an LiTEA coating thicker than 80 MLD cycles commonly could realize long-term cyclability and exhibited a stabilizing stage and a stabilized stage. Their stabilizing stage were several hundreds of Li-stripping/plating cycles. In their stabilized stage, thereafter, their overpotential profiles are stable rectangular waveforms with Li-stripping/plating cycles. To verify these cells' healthy conditions without short circuits, we intentionally made different numbers of holes on separators (Fig. S3) and assembled them a series of symmetric Li||Li cells. The resultant cells were assumed being shorted. The overpotentials of both the shorted bare Li||Li (Fig. S4) and LiTEA-200||LiTEA-200 (Fig. S5) cells was < 1 mV at 2 mA cm^{-2} and < 4 mV at 5 mA cm^{-2}. Apparently, the overpotentials of these shorted cells (Fig. S4 and S5) are much lower than those of the

cells with an LiTEA coating thicker than 80 MLD cycles in Fig. 3. Furthermore, we conducted electrochemical impedance spectroscopy (EIS) measurements on the LiTEA-200‖LiTEA-200 cell cycled for 1700 Li-stripping/plating cycles with a rectangular overpotential waveform (Fig. S6a), the bare Li‖Li cell cycled for 500 Li-stripping/plating cycles (Fig. S6b), the shorted bare Li‖Li cell (Fig. S6c), and the shorted LiTEA-200‖LiTEA cell (Fig. S6d). We observed that the LiTEA-200‖LiTEA-200 cell cycled for 1700 Li-stripping/plating cycles showed two typical semicircles, while the failed bare Li‖Li cell (Fig. S6b) and the shorted cells (Fig. S6c and S6d) showed no cell resistance at all. These results again confirmed that the LiTEA-coated Li symmetric cells with a coating of ≥ 80 MLD cycles were healthy after a long-term cyclability in Fig. 3, although they showed stable low overpotentials.

To better understand the protective effects of the LiTEA coating, we observed the morphological evolutions of the cycled Li electrodes. Fig. 4a shows the surface of four Li electrodes (bare, LiTEA-40, LiTEA-80, and LiTEA-200) after 500 Li-stripping/plating cycles at 2 mA cm^{-2} and 1 mAh cm^{-2}. Both the bare and LiTEA-40 Li electrodes exhibit a porous structure. In contrast, the surface of the LiTEA-80 and LiTEA-200 electrodes were much smoother and denser. The surface changes of the cycled Li electrodes also were compared in Fig. S7, showing that an LiTEA film thicker than LiTEA-80 helped remain the surface smooth and shiny after 500 Li-stripping/plating cycles. We further verified this through observing the cross-sections of the bare, LiTEA-40, LiTEA-80 and LiTEA-200 electrodes after 500 Li-stripping/plating cycles using SEM (Fig. 4b). One can easily observe that, compared to the cross section (Fig. S8) and surface (Fig. S9a) of bare Li metal before cycling, the bare electrode after the cycling has been significantly

corroded with the substantial formation of SEI. In contrast, the LiTEA coatings have evidently protected Li metal from the corrosions. In particular, thicker LiTEA coatings could help remain more Li uncorroded. Very impressively, the cross-section of the LiTEA-200 is nearly intact with very little SEI, and the thickness of the Li layer almost remained unchanged after 500 Li-stripping/plating cycles (Fig. 4b). Thus, we concluded that the thicker the LiTEA coatings are, the better the protection effects could be. Taken together all the afore-discussed results, LiTEA-200 is regarded as the optimal electrode.

Furthermore, we employed XPS depth profiling to investigate the surface composition evolution of four Li electrodes: bare Li (Fig. 4c) and LiTEA-200 electrode (Fig. 4d) after 10 and 50 Li-stripping/plating cycles. Fig. 4c reveals that, after 10 Li-stripping/plating cycles, the F and O signals in the bare Li electrode are considerable and relatively stable with film depth within the sputter time of 1000 s, while the other signals of Li, C, and S are much weaker. These results indicate that there had a very thick SEI layer formed on the bare Li electrode after 10 Li-stripping/plating cycles. The detected F and O signals are most likely from the decomposition of LiTFSI salt and the ether solvent. More details are shown in the high-resolution XPS spectra of the cycled bare Li electrode (Fig. S10a). After 50 Li-stripping/plating cycles, the bare Li electrode shows much stronger F signal, indicating the formation of a thicker SEI layer on Li electrode (Fig. 4c). In sharp contrast, the F signal is almost undetectable on the LiTEA-200 electrode after 10 stripping/plating cycles (Fig. 4d). On the other hand, the O and C signals show similar evolutionary trend, which drop and then level off. It should be pointed out that the evident C and O signals are mainly due to the LiTEA film rather than the decomposed electrolyte compared to that of the cycled bare Li electrodes. This could be verified by the strong C-N and Li-O-C

241 peaks in C 1s and Li 1s spectra of the cycled LiTEA-200 electrode, respectively (Fig.
242 S10b). These results indicate that there had little SEI formed on the LiTEA-200 electrode
243 during cycling. Similar results can be observed on the LiTEA-200 electrode after 50
244 stripping/plating cycles (Fig. 4d). This further verifies that the LiTEA MLD film is
245 chemically stable and serves as an exceptional protective film over Li electrodes in the
246 ether electrolyte. This is consistent to the results of Fig. 4a and 4b. More details are
247 shown in the high-resolution XPS spectra of the cycled LiTEA-200 electrode (Fig. S10b).

248 To further demonstrated the protective effects of this novel LiTEA coating, we conducted
249 a very interesting comparative study under an extremely high areal capacity, 48 mAh cm-
250 ^{2}, in which an LiTEA-200||LiTEA-200 cell and a bare Li||Li cell were comparatively
251 performed an extremely long 24-h Li-stripping on one Li electrode (an extremely long
252 24-h plating occurred simultaneously on the opposing electrode) at a current density of 2
253 mA cm^{-2}. A similar study was conducted in our previous study [1]. As shown in Fig. 5a,
254 the bare Li electrode after the 24-h stripping was widely covered by craters (as circled by
255 dashed lines) and bumps (or highlands, the areas other than the circles) (Fig. 5a(i)), which
256 are partially enlarged in (Fig. 5a(ii)). The highlands are smooth while the craters contain
257 many porous structures (Fig. 5a(iii) and (iv)). Look carefully, one can identify that the
258 highland areas are intact parts of the pristine Li surface area while the craters are the
259 stripped parts. We believe that the porous structures (Fig. 5a(iii) and (iv)) in the craters
260 are the stripping residuals, i.e., the SEI layer. The similar results have been reported in
261 our recent study [1]. As we explained previously, the craters have stripped Li first and
262 then the highlands became the new areas for Li-stripping. This had led to a non-uniform
263 stripping process on bare Li electrodes. Consequently, the stripping areas might change

with time [1]. In addition, the opposite bare Li after a 24-h plating process was also observed (Fig. 5b). A huge amount of dendritic Li has been deposited on the original Li surface (Fig. 5b(i)). Moreover, it could be seen from Fig. 5b(ii) that the deposited Li was separated from the originally bare Li which was flat and smooth (Fig. 5b(iii)), while the deposited Li was in micron-sized dendritic structures (Fig. 5b(iv)). The separation of the bare Li surface and the dendritic structures was caused by the SEI layer formed on both of them. The formation of this SEI layer consumed Li and the electrolyte. In sharp contrast, the surface of the LiTEA-200 electrode after 24-h stripping remained extremely clean and has no craters and bumps observed. Additionally, we also noticed that there were many fractures on the LiTEA coating (Fig. 5c). The fracture gaps between the broken pieces of the LiTEA coating are ~1 μm. The opposite LiTEA-200 electrode after 24-h plating (Fig. 5d) was also nearly clean and smooth with a few of dendritic Li sporadically. These results are very compelling. They indicate that Li could be deposited underneath the LiTEA MLD coating. In other words, the LiTEA coating are Li-ion-conducting but electronically insulating.

We further examined the surface of the bare Li and the LiTEA-200 electrodes after one 48-h Li-stripping/plating cycle (i.e., a 24-h stripping followed by a 24-h plating). It was observed that the bare Li electrode after a 48-h Li-stripping/plating cycle (Fig. 6a) was covered with a thick porous layer of Li dendrites, which is similar as the morphology shown in Fig. 5b. The opposite bare Li after 48-h Li-plating-stripping (Fig. 6b) has a similar appearance as shown in Fig. 5a, exhibiting numerous craters and highlands. In contrast, the LiTEA-200 electrode after a 48-h Li-stripping/plating cycle (Fig. 6c) was almost clean on the surface and merely decorated with a few of Li dendritic structures as

shown in Fig. 5d. The LiTEA coating was fractured with 1-2 μm gaps (Fig. 6c(iv)). Similarly, the LiTEA-200 electrode after 48-h Li-plating/stripping (Fig. 6d) was very clean and covered with small broken pieces of the LiTEA coating, and only a few of Li dendrites could be observed. Based on all the afore-discussed results, we concluded that bare Li could not realize uniform Li-stripping/plating while the LiTEA MLD coating could uniform Li-stripping/plating. More importantly, the LiTEA coating could provide excellent protection over Li electrodes, ascribed to its ionically conductive and electronically insulating nature. This will be further verified and discussed in a later section.

To study the formation of the LiTEA film fractures in Fig. 5 and 6, we conducted a study through assembling a bare Li||Li cell and an LiTEA-200||LiTEA-200 cell and then opening them without cycling to observe their surface changes. We found that the bare Li electrode after the assembling press changed from an originally flat surface (Fig. S9a) to a waved surface (Fig. S11a). On the other hand, we observed that the LiTEA-200 electrode surface after the press has broken from a smooth surface (Fig. S9b) into a cracked surface (Fig. S11b). All these results clearly indicate that the LiTEA coating was fractured mainly during mechanical assembling but not changed during the Li-stripping/plating cycles. Thus, it is easy to understand that thicker LiTEA films could provide better mechanical protections but might increase resistance for ion-transportation. This was corroborated by the results in Fig. 3, showing a decreasing overpotential with an increasing LiTEA coating less than 200 MLD cycles but an increasing overpotentials with an LiTEA coating larger than 200 MLD cycles.

To confirm the fast-ion conducting nature of the LiTEA coating, we studied the evolution of cell impedance with Li-stripping/plating cycles (Fig. 7). The equivalent circuits are proposed for uncycled and cycled cells. R_b, R_{int}, and R_{ct} are the bulk resistor, the interfacial resistor, and charge transference resistor, respectively [34, 35]. CPE represents a constant phase element and W denotes a Warburg element [34, 35]. Prior to Li-stripping/plating cycles, the uncycled bare Li||Li cell has an impedance of ~220 Ω while the uncycled LiTEA-200||LiTEA-200 cell has an impedance of ~800 Ω due to the LiTEA coating (Fig. 7). However, after the 1st Li-stripping/platting cycle, the R_{int} of the bare Li||Li cell is much larger than that of the LiTEA-200||LiTEA-200 cell. This might be caused by the massive formation of SEI on the bare Li surface. The rapid drop of R_{int} in the bare Li||Li cell after the initial cycle is probably due to the electrode activation [36]. After then, the R_{int} and R_{ct} of the bare Li||Li and LiTEA-200||LiTEA-200 cells are comparable within the first 30 Li-stripping/plating cycles, but the R_{int} and R_{ct} values of the bare Li||Li become evidently larger than those of the LiTEA-200||LiTEA-200 cell after 50 cycles. Moreover, the R_{int} and R_{ct} of the LiTEA-200||LiTEA-200 cell only show very small changes with Li-stripping/plating cycles. These results again confirmed that the LiTEA coatings are very effective in stabilizing the Li interface and thereby reducing cell impedance during the Li-stripping/plating cycles. We also compared the EIS of the LiTEA-200||LiTEA-200 and LiTEA-500||LiTEA-500 cells in Fig. S12. Without cycling, the LiTEA-500||LiTEA-500 cell (Fig. S12b) presents much larger R_{int} and R_{ct} than the LiTEA-200||LiTEA-200 cell (Fig. S12a), indicating that a thinner LiTEA film could achieve a higher ionic conductivity. This trend was further confirmed by the EIS after different cycles (Fig. S12c and d), in which the LiTEA-200||LiTEA-200 cell always

shows a smaller impedance. The results also explain the smaller overpotentials of the LiTEA-200 electrode compared to the electrodes with thicker coatings, i.e., LiTEA-300, LiTEA-400, and LiTEA-500.

Motivated by the superior protection effects of the LiTEA coating on Li electrodes in Li||Li symmetric cells, we further investigated these beneficial effects in Li||NMC full cells. Besides some bare NMC811 electrodes, we also coated some NMC811 electrodes conformally with an Li_2S film of 20 ALD cycles, which was named as **Li_2S-20**. We then assembled three cells: bare Li||NMC811, LiTEA-200||NMC811, and LiTEA-200||Li_2S-20 and studied their cyclability in the voltage range of 3.0 – 4.3 V (Fig. 8a). These cells were first tested at 0.2 C (1 C = 200 mA g^{-1}) for 2 charge/discharge cycles and then they were cycled at 1 C for 300 charge/discharge cycles. The bare Li||NMC811 cell dropped to a capacity retention of 80% in ~100 charge/discharge cycles and the LiTEA-200||NMC811 cell extended to the sustainability of 80% capacity retention to ~150 charge/discharge cycles. Very compellingly, the LiTEA-200||Li_2S-20 cell enabled a sustainability of 80% capacity retention after 210 cycles, accounting for a cyclability two times higher than that of the bare Li||NMC811 cell. After 80% capacity retention, particularly, the LiTEA-200||Li_2S-20 cell exhibited a much slower capacity dropping rate, 0.29%/cycle (210-300 cycles) vs. 0.63%/cycle (150 – 300 cycles) for the LiTEA-200||NMC811 cell and 0.92%/cycle (100 – 175 cycles) for the bare Li||NMC811 cell. Comparing their first charge/discharge profiles at 1 C (Fig. S13a), the bare Li||Li, LiTEA-200||NMC811 and LiTEA-200||Li_2S-20 cells have a discharge capacity of 172, 165, and 161 mAh g^{-1}, respectively. The lower initial capacity might be due to both the ALD and MLD coatings. However, the LiTEA-200||Li_2S-20 cells could still sustain a much higher discharge

355 capacity of 97 mAh g^{-1} after 300 cycles, accounting for a capacity retention of > 60%. In
356 contrast, both the bare Li||Li and LiTEA-200||NMC811 cells only retained a capacity
357 retention of ~25%. It indicates that, in addition to the LiTEA coating on the Li anode, the
358 ALD Li_2S coating on the NMC cathode also played a very critical role in the
359 performance of the Li||NMC full cells. This could also be verified in Coulombic
360 efficiency (CE) profiles (Fig. S13b). Within 100 cycles, all of three cells have
361 comparable CE of 98%. However, the profiles in the bare Li||NMC811 and LiTEA-
362 200||NMC811 cells have a big fluctuation after 100 and 150 cycles, respectively,
363 corresponding to their worsened cycling performance in Fig. 8a. Very impressively, the
364 CE of the LiTEA-200||Li_2S-20 cell is much more stable and remains constant in 300
365 cycles. These results again confirmed that surface coatings on both anodes and cathodes
366 can synergistically improve the performance of Li||NMC full cells. In addition, we
367 examined the surface changes of NMC cathodes (Fig. S14a) and Li anodes (Fig. S14b)
368 after 300 charge-discharge cycles. One can observe that the Li_2S-coated NMC cathode
369 shows much fewer cracks and the LiTEA-coated Li anodes retained a smoother and
370 denser surface. Furthermore, we detected the presence of transition metals, especially Ni
371 on the cycled Li electrodes of these three cells after 300 cycles (Fig. 8b-d. Energy
372 dispersive X-ray spectroscopy (EDX) mapping revealed that the detected Ni contents
373 were 0.25, 0.20, and 0.03 at.%, respectively, for the bare Li||NMC811, LiTEA-
374 200||NMC811, and LiTEA-200||Li_2S-20 cell (Fig. 8b-d). More details have been shown
375 in (Fig. S15). We believed that the dissolution and migration of transition metals might
376 be a reason for the faster performance fading of the bare Li||NMC811 and LiTEA-
377 200||NMC811 cells. First, the loss of active materials in NMC, which is one cause of

capacity fade. Second, the deposited transition metal ions on the Li anodes could be reduced to metals, which might have catalyzed the decomposition of electrolyte [11]. The results are very inspiring, for Li||NMC811 LMBs could achieve the best performance with both the coatings, i.e., the MLD LiTEA coating on Li anode and the ALD Li_2S coating on NMC811 cathode. This is significant for addressing the issues of Li||NMC cells to the largest extend.

Based on the results in this study, we proposed the underlying mechanisms of Li-stripping/plating for the bare Li||Li cell and the LiTEA||LiTEA cell, as illustrated in Fig. 9. The evolution of the cross section of a bare Li electrode is shown in Fig. 9a. An Li chip surface is initially smooth and flat (Fig. 9(a1)) but becomes bumpy after the assembling press (Fig. 9(a2)). Upon contacting with the liquid electrolyte after assembling, the Li chip surface was covered by an SEI layer, due to its reaction with the electrolyte (Fig. 9(a2)). The bumps on the Li chip surface are prone to start an Li-stripping first (Fig. 9(a3)). After the depletion of these surface bumps, the neighboring areas become new bumps and continue the stripping while the former bumps become craters covered by an SEI layer (Fig. 9(a4)). In this way, there are more and more SEI produced and the Li chip surface will not be even in composition and morphology after the stripping process (Fig. 9(a5)). Consequently, the Li-plating can not be uniform in a subsequent plating process. Some sites of the Li chip surface are deposited with more Li, and the deposited Li on these sites is more likely to form dendritic structures (Fig. 9(a6)). At the same time, the produced SEI layer on the Li surface may isolate the deposited Li, leading to the formation of dead Li. Moreover, the formed Li dendritic structures could further exacerbate the formation of SEI on the Li chip surface in the following stripping (Fig.

401 9(a7)). After multiple such Li stripping/plating cycles, the bare Li chip is significantly
402 corroded and consumed, and it is covered with a remarkably thick SEI layer (Fig. 9(a8)).
403 Meanwhile, there is also a massive consumption of the electrolyte. These may eventually
404 lead to a significant increase in cell impedance and overpotential.

405 In contrast, the LiTEA MLD coating can form a uniform protective layer over the Li chip
406 surface (Fig. 9(b1)). After the assembling press, the LiTEA-coated Li chip surface also
407 becomes bumpy (Fig. 9(b2)). During the mechanical press, the LiTEA coating fractures.
408 The fractured areas contact the electrolyte and form an SEI layer. However, the Li chip
409 surface is still dominantly covered by the LiTEA coating, and only a very small fraction
410 of the surface is covered by the SEI layer. As we discussed, the LiTEA coating is
411 electronically insulating and ionically conductive, thereby, the stripping starts from the
412 surface bumps (Fig. 9(b3)) but the Li surface quickly flatten after the depletion of these
413 bumps (Fig. 9(b4)). Due to the homogenous properties of the LiTEA coatings, the
414 following stripping and plating process are very even without any further formation of Li
415 dendrites and SEI (Fig. 9(b5)). Consequently, the LiTEA-coated Li electrodes can realize
416 an extremely long-term cyclability and thus, the cell overpotential can sustain stable with
417 extended stripping/plating cycles. It is worth noting that during the Li-stripping/plating
418 processes, a very thick coating layer (e.g., 180 nm or higher) might compromise the
419 protective effect due to the increased resistance of ion transportation (Fig. S12).

420 **3. Conclusions**

421 In this study, we for the first time developed a novel lithicone, LiTEA using MLD, which
422 can be deposited at moderate temperature of 150 °C with a decent average GPC of ~3.6
423 Å cycle^{-1}. Very encouragingly, this LiTEA MLD coating showed exceptional protective

effects on Li electrodes, i.e., remarkable suppression of Li dendrites and SEI formation. We revealed that this LiTEA coating is electrically insulating and ionically conductive. This enabled Li anodes for long-term Li-stripping/plating cyclability in Li‖Li symmetric cells. Furthermore, we demonstrated that this LiTEA MLD coating could evidently mitigate the performance fading of Li‖NMC811 full cells and best extend the cyclability of Li‖NMC811 cells by combining an ALD coating on the NMC811 cathode. Therefore, this study is significant for us to develop lithium metal batteries, using the two emerging techniques of ALD and MLD.

4. Experimental methods

4.1. MLD processes

Using a commercial MLD system (Savannah 200, Ultratech Inc., MA, USA) with argon (Ar) as the carrier gas, the MLD process of LiTEA lithicone has been developed in this study. LTB (Sigma-Aldrich, USA) as the Li source was preheated in a bubbler at 150 °C for a sufficient vapor supply, while TEA (Sigma-Aldrich, USA) was maintained in stainless steel cylinders at 150°C. This MLD system was integrated with an Ar-filled glove box (having an oxygen and water level lower than 1 ppm), and this integration makes the MLD system feasible for many air-sensitive materials. The timing sequence of a single MLD cycle was typically in a sequence of t_1 - t_2 - t_3 - t_4, corresponding to the LTB dose, the first Ar purge, the TEA dose, and the second Ar purge, respectively. The precursor dosing time of both t_1 and t_3 was optimized as 5 s, while the purge time of t_2 and t_4 was optimized as 60 s. During the MLD process, the Ar gas flow was remained at 20 sccm. Li chips were uniformly coated with LiTEA films with different MLD cycles

446 The MLD process has been studied using an *in situ* QCM. The QCM measurements were
447 conducted using a gold sensor crystal (Inficon, USA) and enabled the visualization of the
448 MLD growth in a time-resolved mass change in ng cm^{-2}. To establish a repeatable QCM
449 surface for studying the MLD process, we pre-deposited an Al_2O_3 layer on the QCM via
450 ALD, using trimethylaluminum (TMA) and water as precursors with the timing sequence
451 0.05 - 10 - 0.05 - 10 s.

452 *4.2. NMC electrode preparation*

453 The NMC811 electrode laminates in this study contain 86 wt% NMC811 powder (MSE
454 Supplies, USA), 7 wt% polyvinylidene fluoride (PVDF, HSV900, MTI Corporation,
455 USA), 7 wt% carbon black (Timical Super C65). To fabricate the laminates, a slurry was
456 first prepared by mixing NMC811 powders, PVDF, and carbon black with a suitable
457 amount of 1 methyl-2-pyrrolidinone (NMP, 99.5%, SigmaAldrich) homogenously using a
458 mixer (THINKY, AR-100). Then, the slurry was cast on Al foils. The resultant NMC
459 laminates were first vaporized completely in air and further dried in vacuum at 100 °C for
460 10 h. The mass loading of the as-prepared NMC811 is ~7.0 mg cm^{-2}.

461 *4.3. Li_2S ALD coating on NMC811 cathodes*

462 The Li_2S ALD process has been reported in our previous studies [15, 37]. In this work,
463 both the Li_2S ALD process and the LiTEA MLD process were performed using the same
464 system. The ALD-Li_2S coating was deposited on prefabricated NMC811 laminates
465 directly, using LTB and hydrogen sulfide (4 at% H_2S balanced by Ar, Airgas) as
466 precursors. To supply sufficient vapor, the solid LTB was heated to 150 °C in a stainless
467 steel bubbler. A single cycle of the Li_2S ALD was consisted of four successive steps: (1)
468 a 5 s dose of LTB, (2) a 10 s purge, (3) a 0.5 s dose of H_2S, and (4) a 10 s purge. NMC

electrodes were conformally coated with Li_2S films for 20 ALD cycles (which is the optimal one reported in our previous study [15]). The resultant Li_2S-coated NMC811 was named as **Li_2S-20**.

4.4. Material characterization

We deposited LiTEA films over N-GNS (ACS Material, USA), Si wafers (UniversityWafer, USA), steel plates, and Li chips (MSE Supplies, USA). The as-grown LiTEA films were characterized using a suite of techniques. We determined the GPC of LiTEA films over N-GNS using SEM (XL30, Philips FEI). The morphological characteristics of NMC and Li electrodes were identified using the SEM instrument equipped with EDX. Synchrotron-based XRD was conducted identify the crystallinity of the LiTEA film at the beamline 11-ID-C of the Advanced Photon Source (APS) at Argonne National Laboratory (ANL, IL, USA), having an X-ray wavelength of 0.1173 Å. The composition of LiTEA films on Si wafers was analyzed using XPS (Versa Probe III) with a mono Al K_α source (1486.6 eV) at Arkansas Nano & Bio Materials Characterization Facility at the University of Arkansas (UA, Fayetteville, AR, USA). XPS depth profiling measurements of cycled Li electrodes were conducted using a Thermo Scientific Model K-Alpha XPS system (Thermo Scientific LLC, Madison, Wisconsin) with a monochromatic Al K_α radiation (1486.7 eV) at Center for Integrative Nanotechnology Sciences (CINS) at the University of Arkansas at Little Rock (UALR).

4.4. Electrochemical testing

The electrochemical performance of the bare and LiTEA-coated Li electrodes was first investigated in Li‖Li symmetric cells using CR2032 coin cells. 250-µm thick Li chips were first punched into 7/16" disks and fixed on stainless steel spacers. Then, LiTEA

492 films of different thicknesses were deposited on these Li chips at 150 °C through
493 adjusting MLD cycles. The bare and LiTEA-coated Li chips were assembled into
494 symmetric Li||Li coin cells directly in our integrated MLD-glove box system. The
495 Celgard 2325 membrane was used as the separator, and the electrolyte was 1 M
496 bis(trifluoromethane)sulfonamide lithium salt (LiTFSI, Sigma Aldrich) dissolved in 1,3-
497 dioxolane (DOL) and 1,2-dimethoxyethane (DME) (1:1, v/v) (Sigma Aldrich). Each cell
498 was added 20 μL of the electrolyte (i.e., 1 M LiTFSI in 1:1 DOL/DME). Before
499 electrochemical testing, all the symmetric cells were rested for 20 hours to stabilize their
500 impedance[38]. At room temperature (~25°C), then, the symmetric cells were tested for
501 Li stripping/plating cyclability under two different current densities of 2 and 5 mA cm^{-2}
502 under a fixed areal capacity of 1 mAh cm^{-2}. The effects of the MLD LiTEA-coated Li
503 anodes were further tested in Li||NMC full cells using CR2032 coin cells. The electrolyte
504 used for Li||NMC cells was 1.2 M $LiPF_6$ in ethylene carbonate (EC)/ ethylmethyl
505 carbonate (EMC) (3:7 by weight, Panax Etec Co.). All the assembled Li||NMC cells were
506 rested for 10 h prior to their electrochemical tests at room temperature. The cells were
507 both charged and discharged at 1 C (200 mA g^{-1}) in the voltage range of 3.0 – 4.3 V
508 versus Li/Li^+. The battery cycler was a Neware Battery Testing System (BTS4000,
509 Shenzhen, China). Measurements of electrochemical impedance spectroscopy (EIS, Bio-
510 Logic SP-200, USA) were conducted on Li||Li symmetric cells in the range of 100 kHz to
511 10 mHz with an amplitude voltage of 5 mV.

512 **Acknowledgments**

513 We acknowledge partial support from U.S. Depart of Energy, Office of Science, Office
514 of Basic Energy Sciences with the award number of DE-SC0023439. X.M. also

appreciate the financial support of Chancellor Commercialization Fund and Chancellor Gap Fund from the University of Arkansas, Fayetteville, AR, USA. Portions of this work were performed at Advanced Photon Source (APS), Argonne National Laboratory. This research used resources of the Advanced Photon Source, Office of Science User Facility, supported by the U.S. Department of Energy, Office of Science, Office of Basic Energy Sciences, Argonne National Laboratory under Contract No. DE-AC02-06CH11357.

Author contributions

X.M. directed and supervised the project. X.M. conceived, designed, and was involved all the experimental parts. X. W. performed and was involved in all the experimental parts. J. C. performed the XRD measurements and analyzed the XRD data. K. V. C. performed part of the MLD deposition. F. W. conducted XPS measurements and analyses. X. W. and X. M. co-wrote the manuscript. All authors contributed to discussions and finalization of the manuscript.

Declaration of competing interests

The authors declare no competing interests.

References

[1] X. Meng, K.C. Lau, H. Zhou, S.K. Ghosh, M. Benamara, M. Zou, Molecular Layer Deposition of Crosslinked Polymeric Lithicone for Superior Lithium Metal Anodes, Energy Material Advances, 2021.

[2] X. Meng, Atomic and molecular layer deposition in pursuing better batteries, Journal of Materials Research, (2020) 1-24.

[3] M. Sullivan, P. Tang, X. Meng, Atomic and Molecular Layer Deposition as Surface Engineering Techniques for Emerging Alkali Metal Rechargeable Batteries, Molecules, 2022.

[4] X. Zhang, Y. Chen, F. Ma, X. Chen, B. Wang, Q. Wu, Z. Zhang, D. Liu, W. Zhang, J. He, Regulating Li uniform deposition by lithiophilic interlayer as Li-ion redistributor for highly stable lithium metal batteries, Chemical Engineering Journal, 436 (2022) 134945.

[5] J. He, A. Bhargav, A. Manthiram, Covalent Organic Framework as an Efficient Protection Layer for a Stable Lithium-Metal Anode, Angewandte Chemie, 134 (2022) e202116586.

[6] P. Yan, J. Zheng, J. Liu, B. Wang, X. Cheng, Y. Zhang, X. Sun, C. Wang, J.-G. Zhang, Tailoring grain boundary structures and chemistry of Ni-rich layered cathodes for enhanced cycle stability of lithium-ion batteries, Nature energy, 3 (2018) 600-605.

[7] P. Yan, J. Zheng, M. Gu, J. Xiao, J.-G. Zhang, C.-M. Wang, Intragranular cracking as a critical barrier for high-voltage usage of layer-structured cathode for lithium-ion batteries, Nature communications, 8 (2017) 14101.

[8] S.-M. Bak, E. Hu, Y. Zhou, X. Yu, S.D. Senanayake, S.-J. Cho, K.-B. Kim, K.Y. Chung, X.-Q. Yang, K.-W. Nam, Structural Changes and Thermal Stability of Charged LiNixMnyCozO2 Cathode Materials Studied by Combined In Situ Time-Resolved XRD and Mass Spectroscopy, ACS Applied Materials & Interfaces, 6 (2014) 22594-22601.

[9] R. Jung, M. Metzger, F. Maglia, C. Stinner, H.A. Gasteiger, Oxygen release and its effect on the cycling stability of LiNixMnyCozO2 (NMC) cathode materials for Li-ion batteries, Journal of The Electrochemical Society, 164 (2017) A1361.

[10] H. Wang, W. Ge, W. Li, F. Wang, W. Liu, M.-Z. Qu, G. Peng, Facile fabrication of ethoxy-functional polysiloxane wrapped LiNi0. 6Co0. 2Mn0. 2O2 cathode with improved cycling performance for rechargeable Li-ion battery, ACS Applied Materials & Interfaces, 8 (2016) 18439-18449.

[11] S.S. Zhang, Problems and their origins of Ni-rich layered oxide cathode materials, Energy Storage Materials, 24 (2020) 247-254.

[12] J. He, A. Bhargav, A. Manthiram, In situ grown 1T′-MoTe2 nanosheets on carbon nanotubes as an efficient electrocatalyst and lithium regulator for stable lithium–sulfur full cells, Advanced Energy Materials, 12 (2022) 2103204.

[13] X. Meng, An overview of molecular layer deposition for organic and organic–inorganic hybrid materials: mechanisms, growth characteristics, and promising applications, Journal of Materials Chemistry A, 5 (2017) 18326-18378.

[14] Q. Sun, K.C. Lau, D. Geng, X. Meng, Atomic and molecular layer deposition for superior lithium-sulfur batteries: Strategies, performance, and mechanisms, Batteries & Supercaps, 1 (2018) 41-68.

[15] X. Wang, J. Cai, Y. Ren, M. Benamara, X. Zhou, Y. Li, Z. Chen, H. Zhou, X. Xiao, Y. Liu, High-performance LiNi0. 8Mn0. 1Co0. 1O2 cathode by nanoscale lithium sulfide coating via atomic layer deposition, Journal of Energy Chemistry, 69 (2022) 531-540.
[16] Y. Liu, X. Wang, S.K. Ghosh, M. Zou, H. Zhou, X. Xiao, X. Meng, Atomic layer deposition of lithium zirconium oxides for the improved performance of lithium-ion batteries, Dalton Transactions, 51 (2022) 2737-2749.
[17] X. Wang, J. Cai, Y. Liu, X. Han, Y. Ren, J. Li, Y. Liu, X. Meng, Atomic-scale constituting stable interface for improved LiNi0.6Mn0.2Co0.2O2 cathodes of lithium-ion batteries, Nanotechnology, 32 (2021) 115401.
[18] Y. Liu, X. Wang, J. Cai, X. Han, D. Geng, J. Li, X. Meng, Atomic-scale tuned interface of nickel-rich cathode for enhanced electrochemical performance in lithium-ion batteries, Journal of Materials Science & Technology, 54 (2020) 77-86.
[19] X. Wang, S.K. Ghosh, M. Afshar-Mohajer, H. Zhou, Y. Liu, X. Han, J. Cai, M. Zou, X. Meng, Atomic layer deposition of zirconium oxide thin films, Journal of Materials Research, 35 (2020) 804-812.
[20] J. Cai, Z. Ma, U. Wejinya, M. Zou, Y. Liu, H. Zhou, X. Meng, A revisit to atomic layer deposition of zinc oxide using diethylzinc and water as precursors, Journal of Materials Science, 54 (2019) 5236-5248.
[21] J. Cai, B. Reinhart, P. Eng, Y. Liu, C.-J. Sun, H. Zhou, Y. Ren, X. Meng, Nitrogen-doped graphene-wrapped Cu2S as a superior anode in sodium-ion batteries, Carbon, 170 (2020) 430-438.
[22] K.N. Wood, G. Teeter, XPS on Li-battery-related compounds: analysis of inorganic SEI phases and a methodology for charge correction, ACS Applied Energy Materials, 1 (2018) 4493-4504.
[23] X. Sun, H.-J. Li, N. Ou, B. Lyu, B. Gui, S. Tian, D. Qian, X. Wang, J. Yang, Visible-light driven TiO2 photocatalyst coated with graphene quantum dots of tunable nitrogen doping, Molecules, 24 (2019) 344.
[24] H. Peng, Z. Mo, S. Liao, H. Liang, L. Yang, F. Luo, H. Song, Y. Zhong, B. Zhang, High performance Fe-and N-doped carbon catalyst with graphene structure for oxygen reduction, Scientific reports, 3 (2013) 1765.
[25] X. Hu, L. Liu, Y. Zhang, A. Chen, Preparation of an N-doped mesoporous carbon sphere and sheet composite as a high-performance supercapacitor, Journal of Chemical Research, 45 (2021) 510-518.
[26] R. Sitko, P. Janik, B. Feist, E. Talik, A. Gagor, Suspended aminosilanized graphene oxide nanosheets for selective preconcentration of lead ions and ultrasensitive determination by electrothermal atomic absorption spectrometry, ACS applied materials & interfaces, 6 (2014) 20144-20153.
[27] X. Zhou, Y. Zhang, Z. Huang, D. Lu, A. Zhu, G. Shi, Ionic liquids modified graphene oxide composites: a high efficient adsorbent for phthalates from aqueous solution, Scientific Reports, 6 (2016) 38417.
[28] D. Bar-Tow, E. Peled, L. Burstein, A study of highly oriented pyrolytic graphite as a model for the graphite anode in Li-Ion batteries, Journal of the Electrochemical Society, 146 (1999) 824.
[29] A.A. Pozveh, E. Kowsari, M.M. Hashemi, Z. Mirjafari, Preparation and electromagnetic wave absorption properties of polymer nanocomposites based on new

functionalized graphene oxide iron pentacarbonyl and ionic liquid, Research on Chemical Intermediates, 46 (2020) 1329-1351.
[30] A. Liu, G. Liu, C. Zhu, H. Zhu, E. Fortunato, R. Martins, F. Shan, Solution-Processed Alkaline Lithium Oxide Dielectrics for Applications in n-and p-Type Thin-Film Transistors, Advanced Electronic Materials, 2 (2016) 1600140.
[31] L.J. Rendek, G.S. Chottiner, D.A. Scherson, The reactivity of linear alkyl carbonates toward metallic lithium: X-ray photoelectron spectroscopy studies in ultrahigh vacuum, Journal of the Electrochemical Society, 149 (2002) E408.
[32] H. Wang, K.E. Gregorczyk, S.B. Lee, G.W. Rubloff, C.-F. Lin, Li-containing organic thin film—structure of lithium propane dioxide via molecular layer deposition, The Journal of Physical Chemistry C, 124 (2020) 6830-6837.
[33] H.S. Casalongue, S. Kaya, V. Viswanathan, D.J. Miller, D. Friebel, H.A. Hansen, J.K. Nørskov, A. Nilsson, H. Ogasawara, Direct observation of the oxygenated species during oxygen reduction on a platinum fuel cell cathode, Nature communications, 4 (2013) 2817.
[34] K. Wen, L. Liu, S. Chen, S. Zhang, A bidirectional growth mechanism for a stable lithium anode by a platinum nanolayer sputtered on a polypropylene separator, RSC advances, 8 (2018) 13034-13039.
[35] C. He, J. Liu, J. Cui, J. Li, X. Wu, A gel polymer electrolyte based on Polyacrylonitrile/organic montmorillonite membrane exhibiting dense structure for lithium ion battery, Solid State Ionics, 315 (2018) 102-110.
[36] B. Lei, J. Yang, Z. Xu, S. Su, D. Wang, J. Jiang, J. Feng, A fumed alumina induced gel-like electrolyte for great performance improvement of lithium–sulfur batteries, Chemical Communications, 54 (2018) 13567-13570.
[37] X. Meng, D.J. Comstock, T.T. Fister, J.W. Elam, Vapor-phase atomic-controllable growth of amorphous Li2S for high-performance lithium–sulfur batteries, Acs Nano, 8 (2014) 10963-10972.
[38] Y. Cao, X. Meng, J.W. Elam, Atomic Layer Deposition of LixAlyS Solid-State Electrolytes for Stabilizing Lithium-Metal Anodes, ChemElectroChem, 3 (2016) 858-863.

Figure Captions:

Fig. 1. The growth of LiTEA via MLD. (a) Schematic illustration of the LiTEA MLD process. (b) QCM measurements of the MLD LiTEA in 50 cycles at 150 °C (Inset: the QCM growth of 100-cycle ALD Al_2O_3 prior to the MLD LiTEA growth). (c) The QCM profile of three consecutive MLD LiTEA growth cycles in the stable growth region.

Fig. 2. (a) SEM images of pristine N-GNS and 100-MLD-cycle LiTEA over N-GNS. (b) High-resolution XPS analyses of LiTEA films: Li 1s, N 1s, C 1s, and O 1s spectra.

Fig. 3. Electrochemical evaluations of LiTEA-coated Li electrodes in Li||Li symmetric cells. The Li||Li cells were tested at (a) 2 mA cm^{-2} and (b) 5 mA cm^{-2} with a fixed areal capacity of 1 mAh cm^{-2}.

Fig. 4. Analyses on cycled Li||Li cells. SEM images of (a) the surfaces and (b) the cross-sections of the cycled bare, LiTEA-40, LiTEA-80, and LiTEA-200 electrodes after 500 Li-stripping/plating cycles at 2 mA cm^{-2} and 1 mAh cm^{-2}. XPS depth profiling on (c) bare and (d) LiTEA-200 electrodes after 10 and 50 Li stripping/plating cycles at 2 mA cm^{-2} and 1 mAh cm^{-2}.

Fig. 5. SEM images of the morphological changes of Li electrodes. (a, b) The bare Li electrode and (c, d) the LiTEA-200 electrode after one 24-h stripping (or plating) at 2 mA cm^{-2}.

Fig. 6. SEM of the morphological changes of Li electrodes. (a, b) The bare Li electrode and (c, d) the LiTEA-200 electrode after one 48-h stripping-plating or platting-stripping at 2 mA cm^{-2}.

Fig. 7. EIS measurements of the bare Li‖Li and LiTEA-200‖LiTEA-200 cells before cycling and after different cycles, which have been cycled at 2 mA cm^{-2} and 1 mAh cm^{-2}.

Fig. 8. (a) Cycle performance of Li‖NMC full cells. SEM images and EDX mapping of cycled Li electrodes disassembled from (b) bare Li‖NMC811, (c) LiTEA-200‖NMC811, and (d) LiTEA-200‖Li_2S-20 cells. All cells were cycled at 1 C (1 C = 200 mA g^{-1}) for 300 cycles.

Fig. 9. Schematic illustrations of the proposed mechanisms of Li stripping/plating for bare Li and LiTEA-coated Li. The Li stripping/plating mechanism of (a) the bare Li and (b) the LiTEA-coated Li.

Figures:

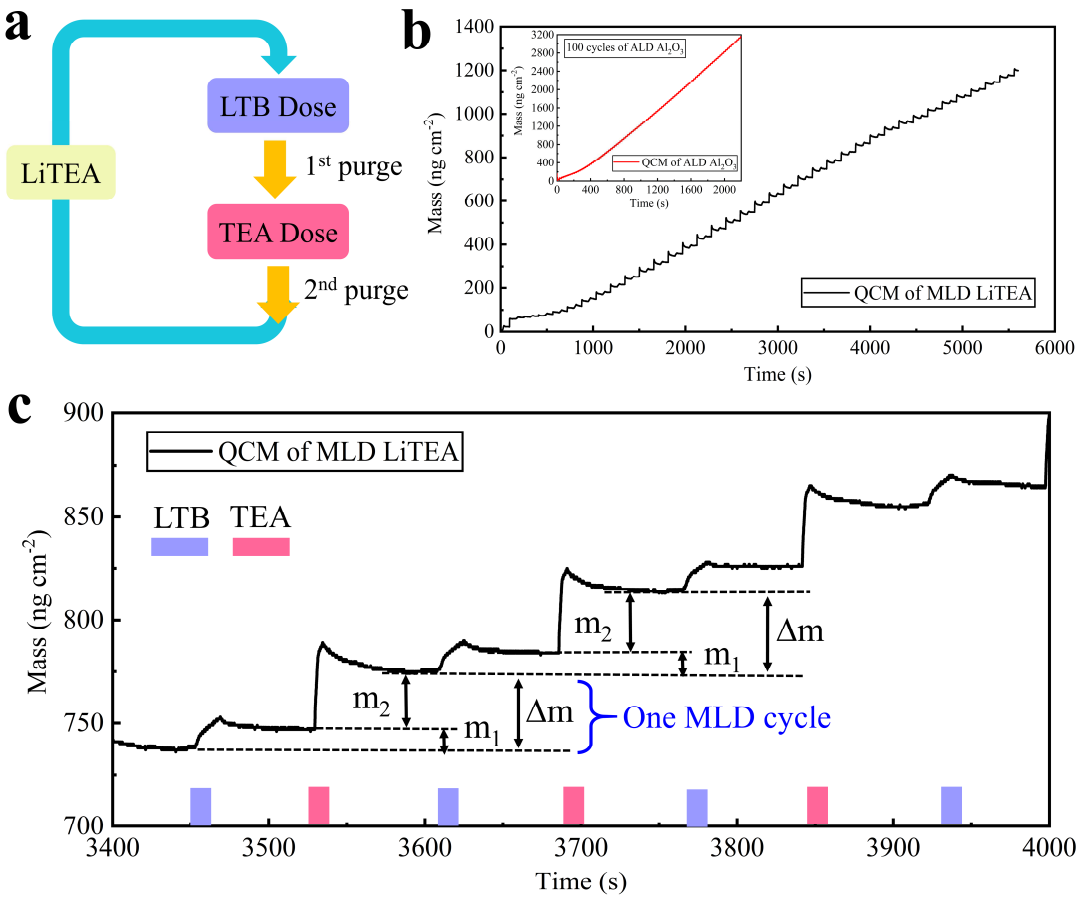

Fig. 1

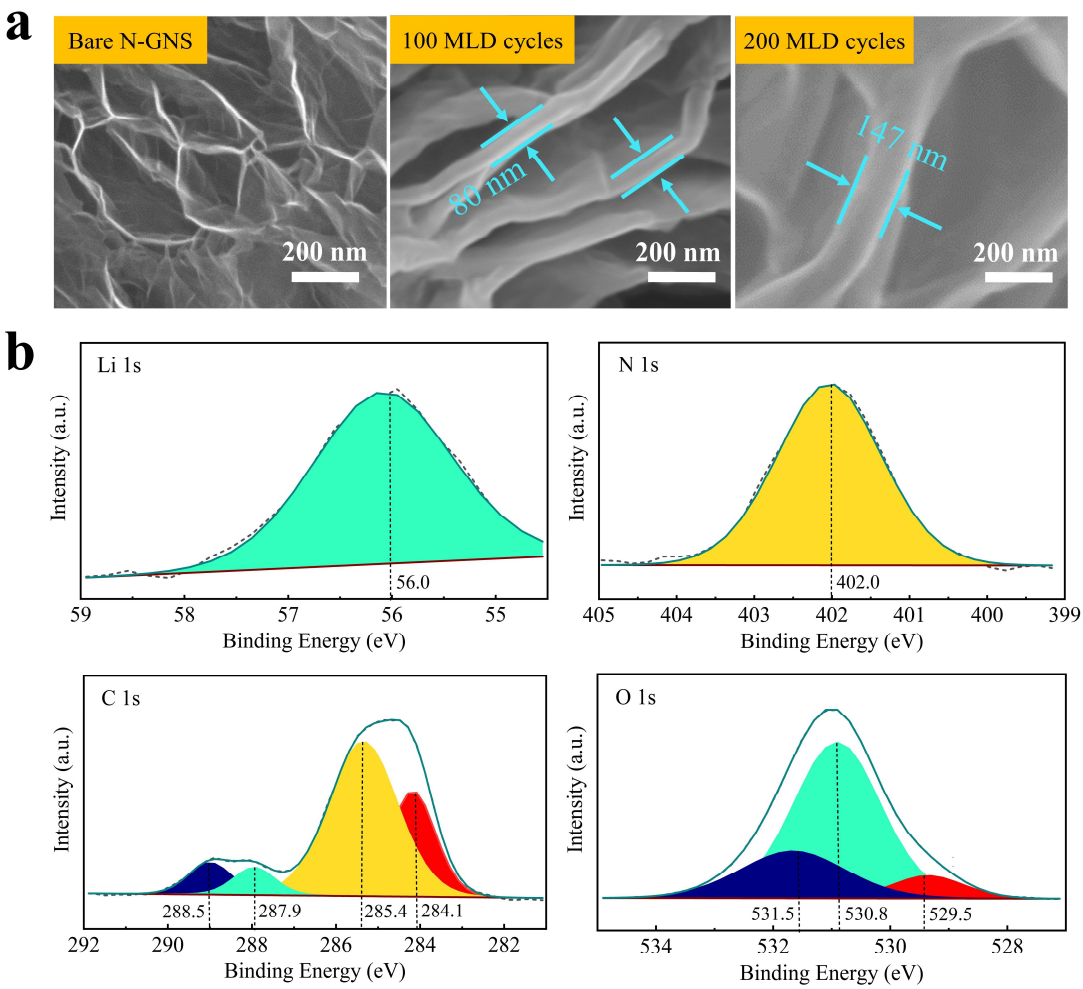

706

707

708 **Fig. 2**

709

710

711

712

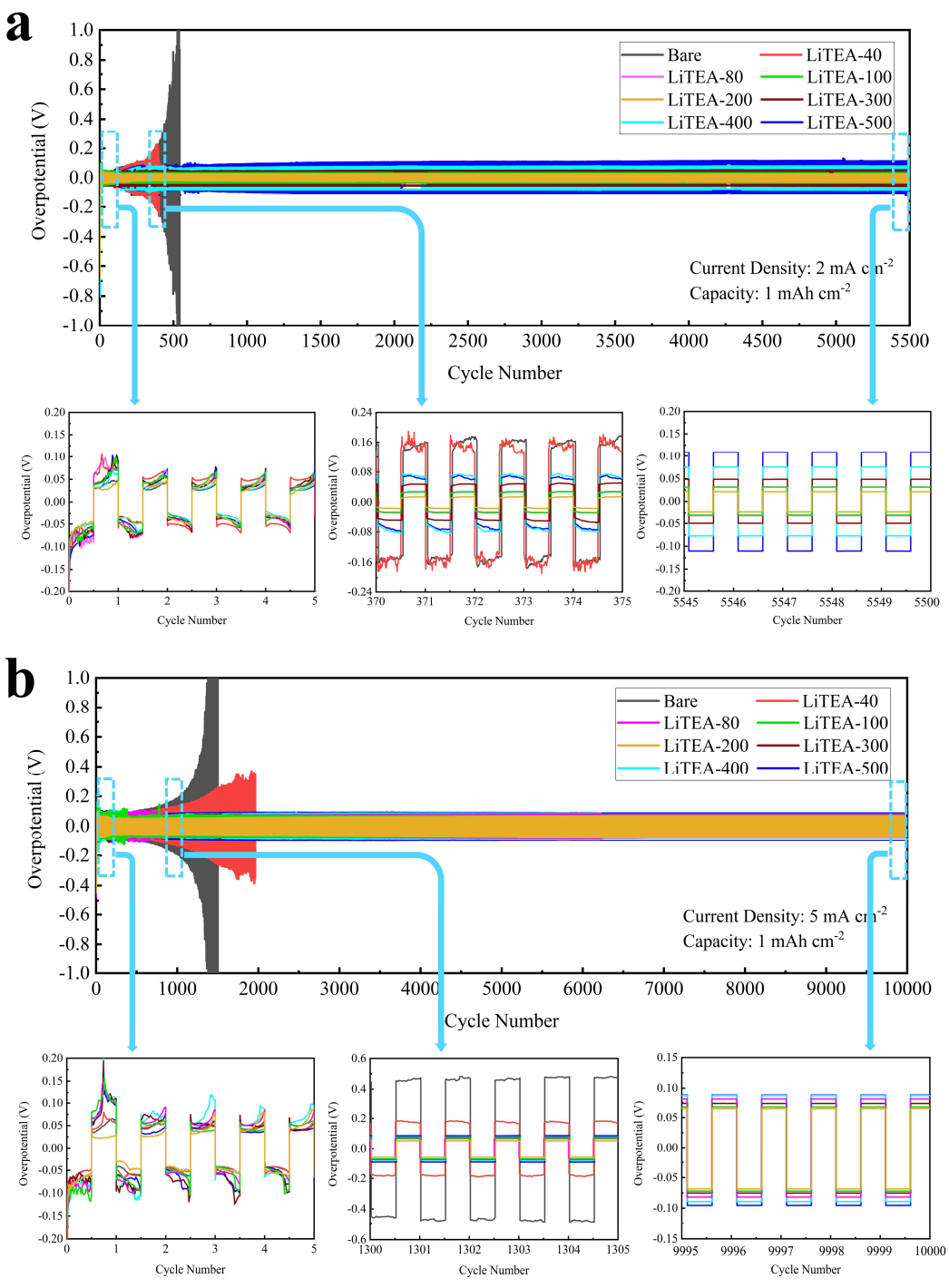
a
Bare
LiTEA-40
LiTEA-80
LiTEA-100
LiTEA-200
LiTEA-300
LiTEA-400
LiTEA-500
Overpotential (V)
Cycle Number
Current Density: 2 mA cm-2
Capacity: 1 mAh cm-2
b
Current Density: 5 mA cm-2
Capacity: 1 mAh cm-2

713

714 **Fig. 3**

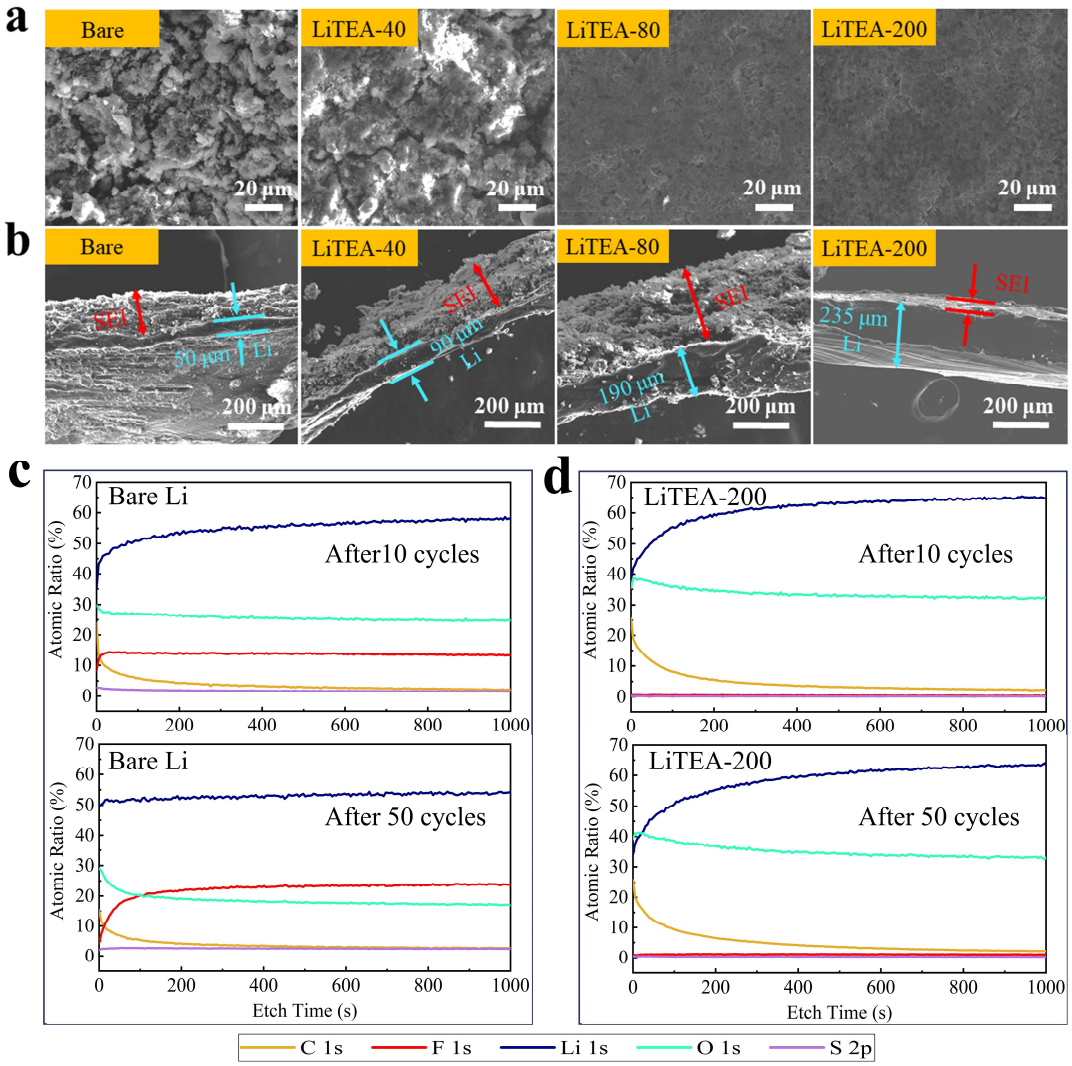

715

716

717 **Fig. 4**

718

719

720

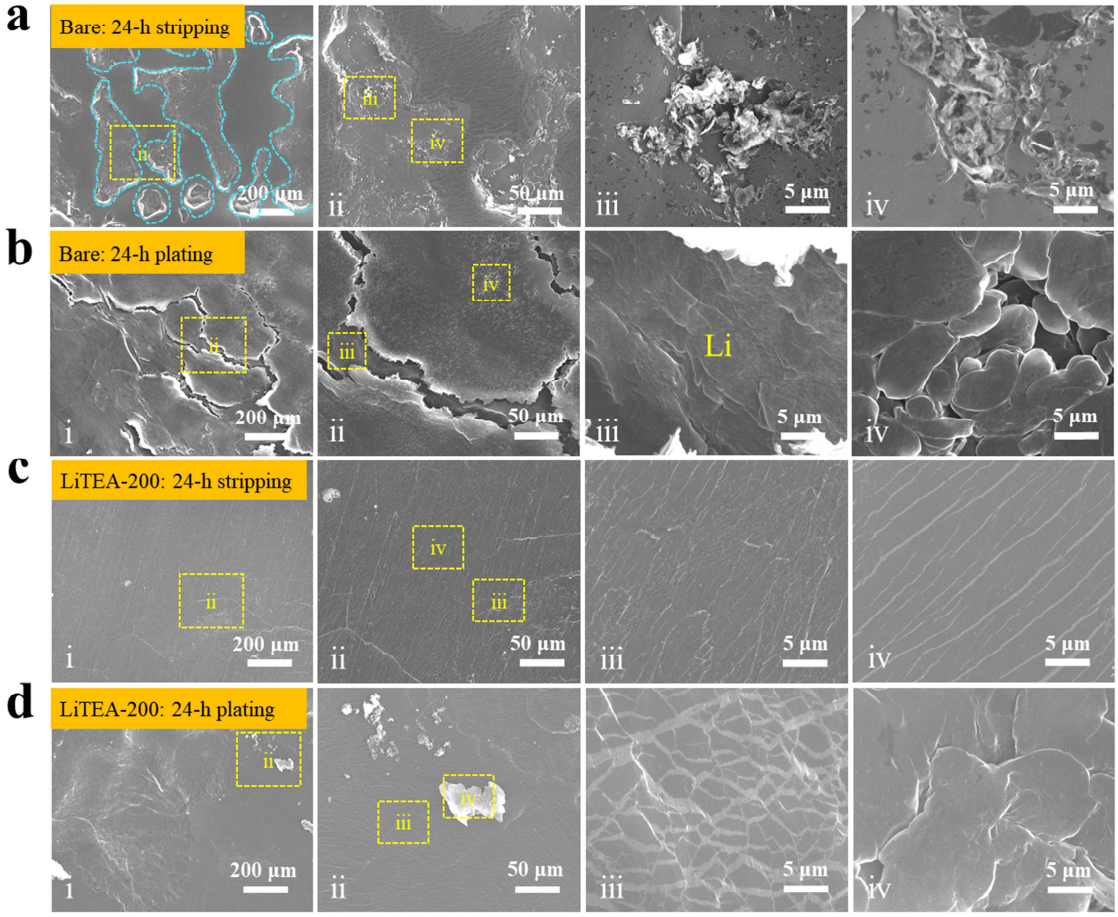

721

722

723 **Fig. 5**

724

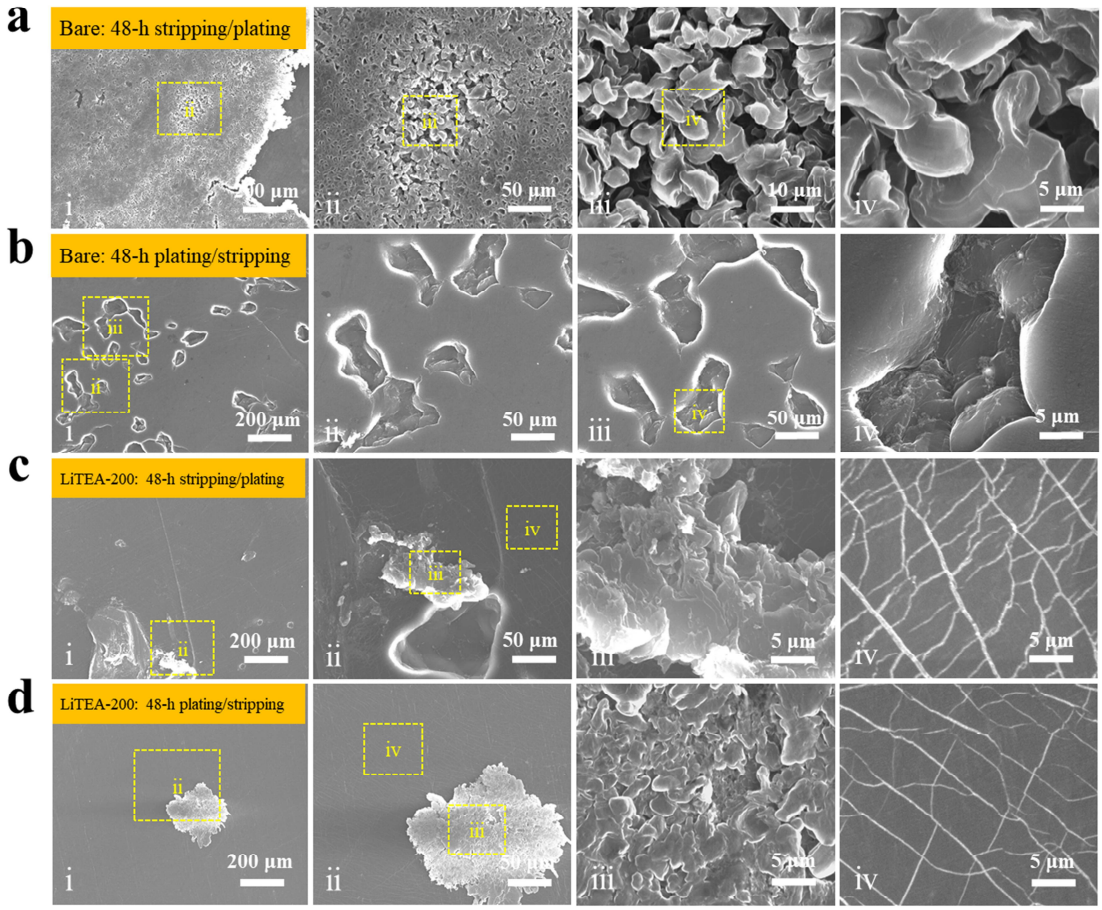
a
Bare: 48-h stripping/plating
200 μm
50 μm
10 μm
5 μm
b
Bare: 48-h plating/stripping
200 μm
50 μm
50 μm
5 μm
c
LiTEA-200: 48-h stripping/plating
200 μm
50 μm
5 μm
5 μm
d
LiTEA-200: 48-h plating/stripping
200 μm
5 μm
5 μm

Fig. 6

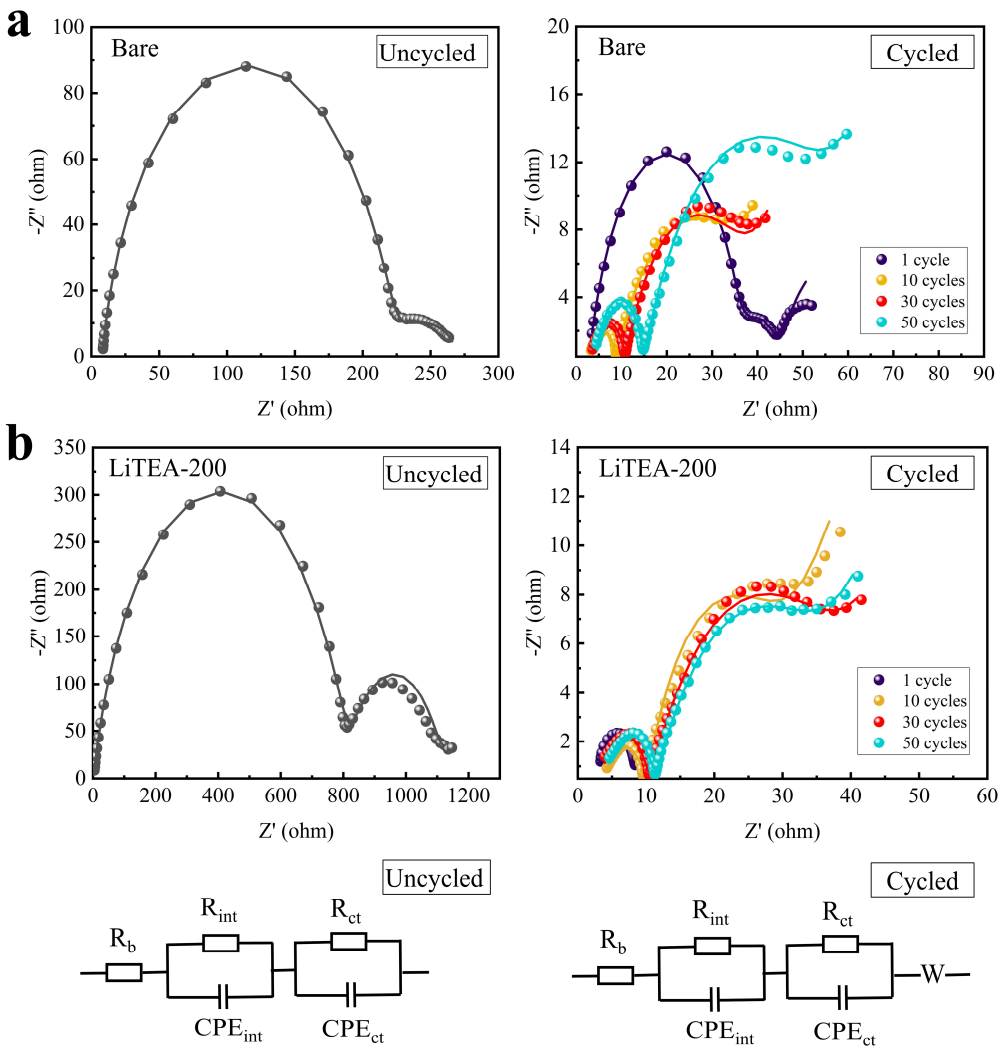

733

734

735 **Fig. 7**

736

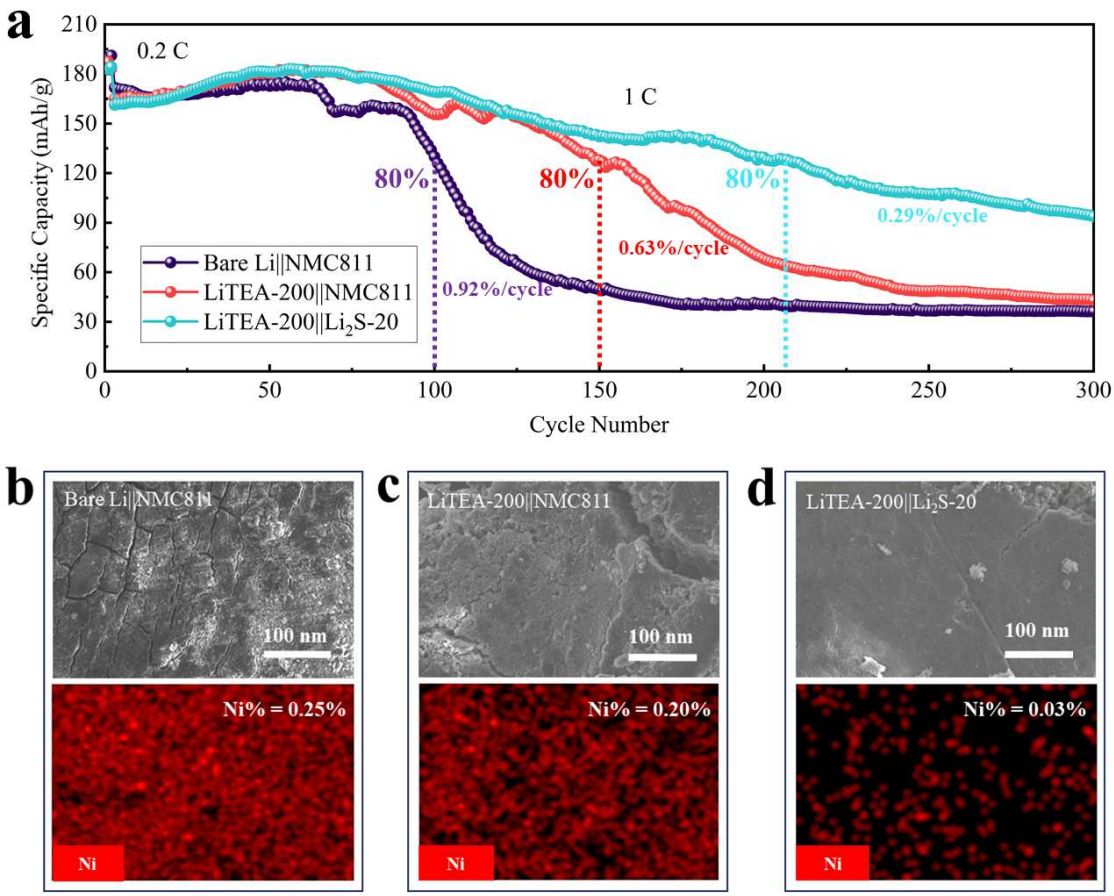
a
0.2 C
1 C
Specific Capacity (mAh/g)
Cycle Number
80%
80%
80%
0.92%/cycle
0.63%/cycle
0.29%/cycle
Bare Li||NMC811
LiTEA-200||NMC811
LiTEA-200||Li2S-20
b
Bare Li||NMC811
100 nm
Ni% = 0.25%
Ni
c
LiTEA-200||NMC811
100 nm
Ni% = 0.20%
Ni
d
LiTEA-200||Li2S-20
100 nm
Ni% = 0.03%
Ni

Fig. 8

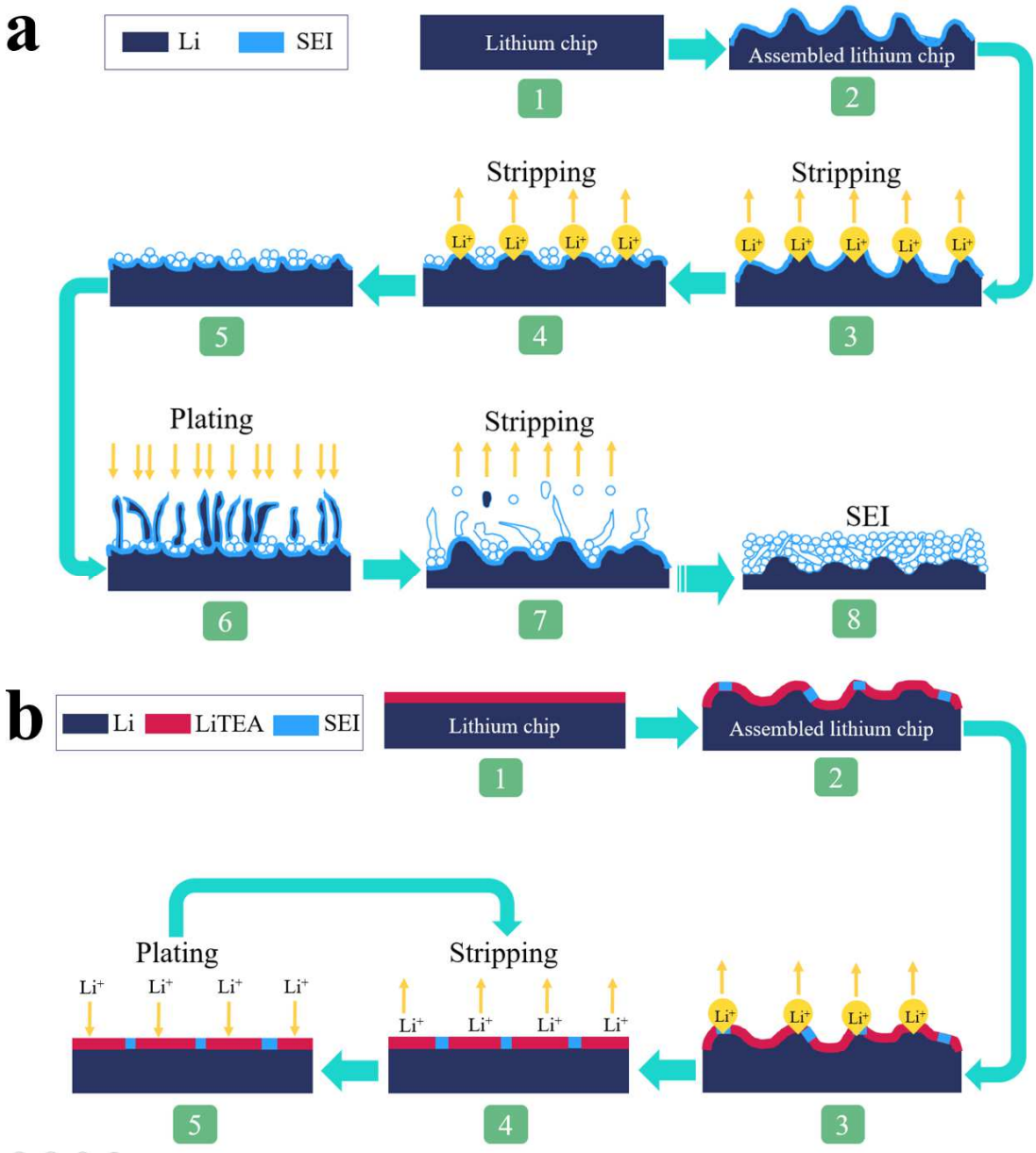

745

746

747 **Fig. 9**

748

The protective mechanisms of LiTEA MLD coating

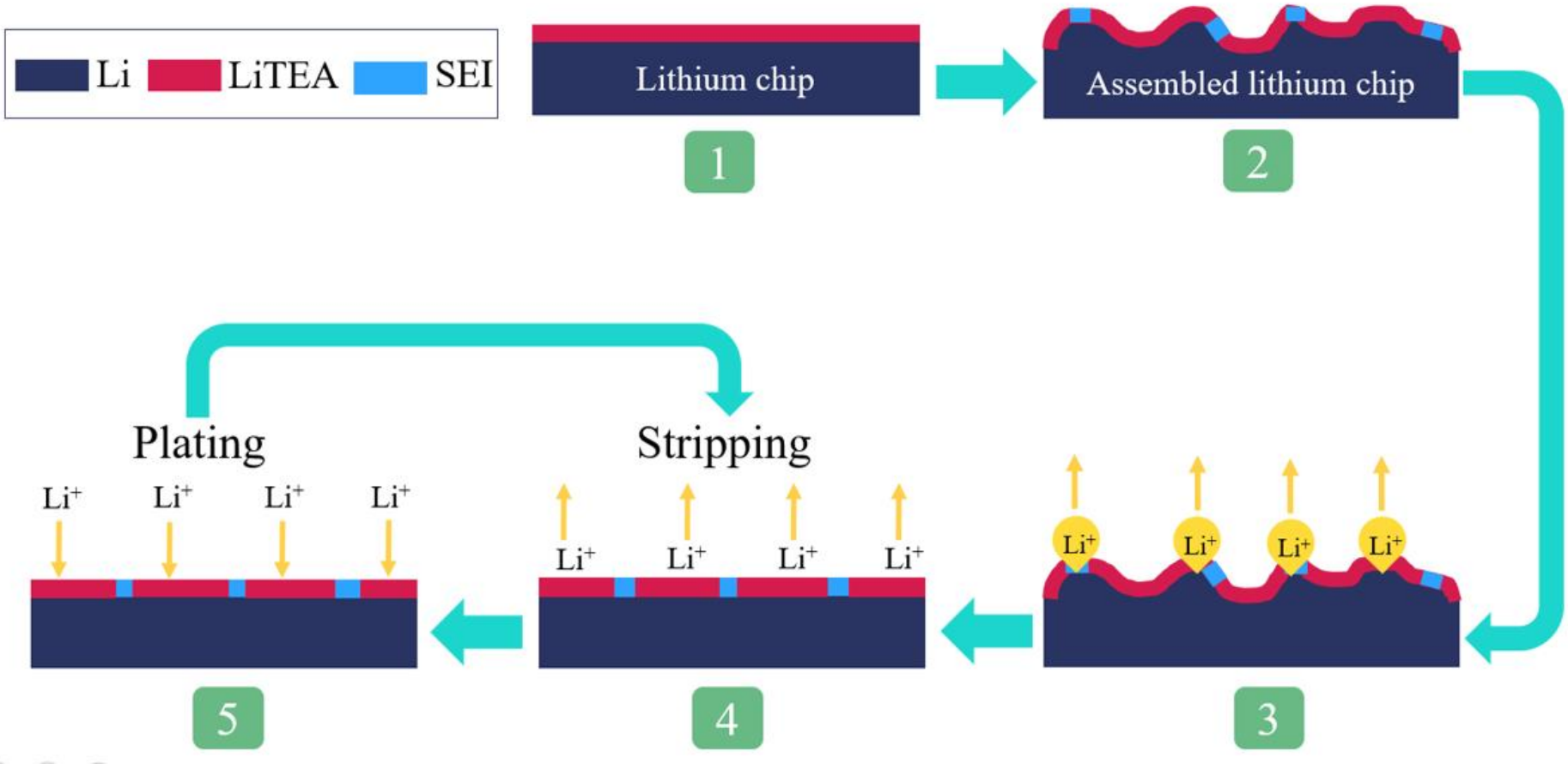

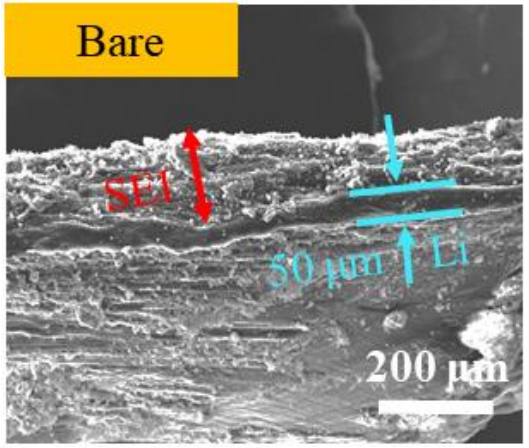

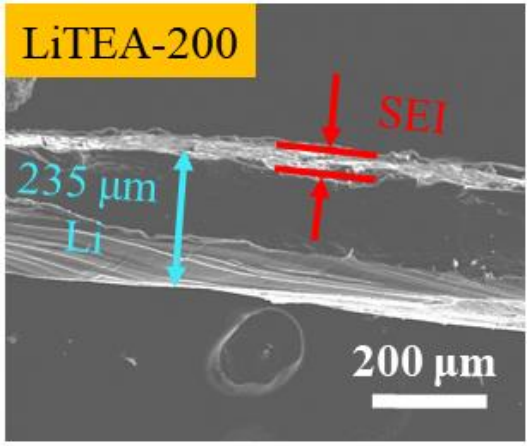

Graphical abstract

The LiTEA MLD coating showed exceptional protective effects on Li electrodes during long-term Li-stripping/plating cycles, i.e., remarkable suppression of Li dendrites and SEI formation.